Journal of the Korean Society of Marine Environment & Safety
Research Paper
Vol. 25, No. 5, pp. 617-626, August 31, 2019, ISSN 1229-3431(Print) / ISSN 2287-3341(Online) https://doi.org/10.7837/kosomes.2019.25.5.617

Optimal Gas Detection System in Cargo Compressor Room of Gas Fueled LNG Carrier

Sang-Won Lee* · Yude Shao** · Seung-Hun Lee** · Jin-Uk Lee*** · Eun-Seok Jeong*** · Ho-Keun Kang****†

* Department of Ship Hull Piping Design, Daewoo Shipbuilding & Marine Engineering Co., Ltd.., Kyungnam, Korea
** Department of Marine System Engineering, Graduate School, Korea Maritime & Ocean University, Busan, Korea
*** Department of Ship Operation, Korea Maritime & Ocean University, Busan, Korea
**** Division of Marine System Engineering, Korea Maritime & Ocean University, Busan, Korea

가스추진 LNG 운반선의 가스 압축기실에 설치된 가스검출장치의 최적 배치에 관한 연구

이상원* · 소예덕** · 이승훈** · 이진욱*** · 정은석*** · 강호근****†

* 대우조선해양, ** 한국해양대학교 대학원, *** 한국해양대학교 선박운항과, **** 한국해양대학교 기관시스템공학부

Abstract : *This study analyzes the optimal location of gas detectors through the gas dispersion in a cargo compressor room of a 174K LNG carrier equipped with high-pressure cargo handling equipment; in addition, we propose a reasonable method for determining the safety regulations specified in the new International Code of the Construction and Equipment of Ships Carrying Liquefied Gases in Bulk (IGC). To conduct an LNG gas dispersion simulation in the cargo compressor room-equipped with an ME-GI engine-of a 174 K LNG carrier, the geometry of the room as well as the equipment and piping, are designed using the same 3D size at a 1-to-1 scale. Scenarios for a gas leak were examined under high pressure of 305 bar and low pressure of 1 bar. The pinhole sizes for high pressure are 4.5, 5.0, and 5.6mm, and for low pressure are 100 and 140 mm. The results demonstrate that the cargo compressor room will not pose a serious risk with respect to the flammable gas concentration as verified by a ventilation assessment for a 5.6 mm pinhole for a high-pressure leak under gas rupture conditions, and a low-pressure leak of 100 and 140 mm with different pinhole sizes. However, it was confirmed that the actual location of the gas detection sensors in a cargo compressor room, according to the new IGC code, should be moved to other points, and an analysis of the virtual monitor points through a computational fluid dynamics (CFD) simulation.*

Key Words : *LNG carrier, Gas detection, BOG, New IGC codes, LNG fueled system, Gas dispersion, Safety*

요 약 : 본 연구는 가스추진 174K급 LNG 운반선의 가스 압축기실에서 발생하는 가스누출 모사를 통해 가스탐지기의 최적 위치를 분석하였으며, 새로 개정된 IGC 코드에 명시된 안전규정을 만족하는 합리적인 방법도 함께 제안하였다. 가스압축기실에서의 LNG 가스누출 수치해석을 위해, 실제 ME-GI 엔진이 장착된 174K급 LNG 운반선의 압축기실 형상과 장비, 배관의 배치와 같은 치수로 3D 설계되었다. 가스누설에 대한 시나리오는 305 bar의 높은 압력과 1 bar의 낮은 압력을 적용하여 진행하였다. 고압용 핀홀의 크기는 4.5, 5.0, 5.6 mm이고 저압용은 100, 140 mm이다. 해석 결과, 5.6 mm 핀홀(고압)과 100, 140 mm 핀홀(저압) 상태의 누출에 대한 환기평가에서 가연성 가스농도는 심각한 위험이 없음을 확인하였다. 그러나 개정된 IGC 코드에 따라 설치된 압축기실의 가스 감지 센서의 실제 위치는 다른 지점으로 이동해야 하고, 측정 지점이 현 규정에서 요구하는 것보다 더 추가되어야 함을 확인하였다.

핵심용어 : LNG 운반선, 가스 검출, BOG, 신규 IGC 코드, LNG 연료 공급 시스템, 가스 분산, 안전

* First Author : sangwon@dsme.co.kr, 055-735-4335
† Corresponding Author : hkkang@kmou.ac.kr, 051-410-4260

1. Introduction

Owing to recent environmental issues, the IMO has adopted regulations to address the emission of air pollutants from ships and has adopted mandatory energy efficiency measures to reduce the emissions of greenhouse gases from international shipping under Annex VI of the IMO's pollution prevention treaty (MARPOL). In addition, IMO regulates air pollutants from international shipping, particularly nitrogen oxide (NOx) and sulphur oxide (SOx) emitted from ships.

To comply with recent IMO requirements, LNG fuel has entered limelight as an effective solution (Bengtsson et al., 2011; Burel et al., 2013; Hoenders, 2013). Therefore, many vessels equipped with LNG fuel are being built in the world. LNG can be considered the most environmentally friendly fossil fuel because it has the lowest CO_2 emissions per unit of energy, and because it is suitable for use in high-efficiency combined cycle power stations (IMO, MEPC.212(63), 2012a; 2012b).

For an equivalent amount of heat, the burning of natural gas produces about 30 % less CO_2 than the burning of petroleum, and about 45 % less CO_2 than the burning of coal. However, LNG is easily vaporized to 600 times the volume, and changes into a flammable gas when mixed with air. The flammable range is about 5 – 15 vol%. (GECF, Gas Basic, 2013)

Most traditional classification rules are detailed prescriptive requirements for specific types of equipment or designs that must be adopted or functional requirements that must be attained, for all installations classed under the rules. This gives very clear instructions on how to design these aspects of the installation. It implies that the responsibility for safety in these areas rests mainly with the classification society because the designer is simply required to satisfy the application rules. In general, such rules have been developed by expert judgment, responding to previous accident experience. They are only rarely based on a risk assessment, and do not themselves satisfy the requirements of performing a risk assessment (Chang et al., 2008).

Many high-pressure gas-fueled LNG vessels which are combined with a high-pressure fuel gas compressor or high-pressure pump/vaporizer have been built because LNG fuel is regarded as environmentally friendly and satisfies the IMO requirements; however, there are many reasons to examine the safety requirements such as for a gas leakage, explosion, or fire. Because conventional LNG carriers applied by the IGC code have been under sail for a long period of time, there are many adequate safety regulations. However, in LNG fueled vessels including newly built LNG carriers, there are some incomplete safety regulations because LNG powered vessels applied by the new IGC code do not have sufficient references. Most safety regulations of the new IGC codes are applied in accordance with the requirements of the IGC codes, and thus there are many inadequate regulations for preventing the risk elements in LNG fueled vessels. In particular, the gas detection system applied in the machinery room based on the IGF and new IGC codes simply defines the number of gas detectors. There are no rules for their locations, and thus the gas detectors are installed based on an agreement among the ship owners, shipyard, and classification societies. The minimum number of detectors in a machinery room (cargo compressor room) by the new IGC code is three, but there are no rules for its detection points. Therefore, ship owners do not rely heavily on the detection system of the new IGC code.

Recently, 174K ME-GI LNG carriers used for carrying cryogenic liquefied natural gas at -163℃ have been designed, and nearly 30 vessels with typical cargo handling equipment and piping arrangement have been constructed according to the new IGC code. Because the vessels use LNG as fuel, there are many reasons to examine their safety requirements such as for a gas leakage, explosion, or fire (MAN B&W Diesel, 2006; Paltrinieri et al., 2015). Thus, it is positively necessary to identify the optimum number of gas detection sensors and their locations to prevent or mitigate a gas accident. In this paper, we present a reasonable method for identifying the risk of an explosion and to determine the optimal location of gas detecting devices. To examine the above-stated points, an LNG gas dispersion simulation for a high/low-pressure leakage in the cargo compressor rooms of 174K ME-GI LNG carriers was carried out according to the volume flow rate of the leak and the new IGC code. The ventilation capability and the locations of gas detection sensor were verified through comparison between actual gas detection sensor and virtual monitor points.

2. Methodology

2.1 System configuration

To conduct the LNG gas dispersion simulation in a cargo compressor room, a 174K LNG vessel built by DSME in Korea was selected to have the same 3D size, not only for the equipment but also for the compressor room geometry, and the initial conditions and leak scenario were defined according to the pinhole sizes.

Fig. 1. Layout in cargo compressor room on the first deck of 174K LNG vessel equipped with a high-pressure fuel gas compressor for the ME-GI main engines and re-liquefaction equipment with leak points of HP pump/vaporizer discharge pipe.

Fig. 1 shows the general arrangement of an ME-GI and re-liquefaction system in the cargo compressor room of an LNG vessel. The main fuel gas consumers are two sets of an ME-GI main engine and four sets of a dual fuel generator engine (DFG) located in the engine room. Fuel gas of 305 bar is supplied by a high-pressure fuel gas compressor or high-pressure pump/vaporizer. Re-liquefaction equipment located in the cargo compressor room, and a gas combustion unit (GCU), which is located in the engine room, is used in the case of excessive BOG treatment.

This research analyzes the optimal gas detecting system through the gas leak and dispersion of both a high-pressure leak and a low-pressure leak according to the varying scenarios that can occur. The ventilation capability in the room and the gas detection sensor locations were verified through a comparison between a real gas detection sensor and the virtual monitor points.

2.2 Leak scenarios and boundary conditions

The new IGC code (2016) specifies that artificial ventilation inlet and outlets shall be arranged to ensure sufficient air movement through space to avoid the accumulation of flammable, toxic, or asphyxiant vapors, and to ensure a safe working environment. In addition, the ventilation system shall have a capacity of no less than 30 changes of air per hour, based upon the total volume of the space (Kang, 2012). According to the new IGC code 13.6.12, the rule requirement specifies that for every installation, the number and positions of the detection heads shall be determined with due regard to the size and layout of the compartment. Therefore, we should consider the reasonable means of achieving the safety regulations, as well as the number of gas detectors and their location, specified in the code.

To realize the gas dispersion simulation, the actual physical properties of LNG gas were applied, as defined in Table 1. The LNG consumed in the model ship was provided by the Korea Gas

Table 1. Numerical conditions for gas dispersion in gas compressor room of 174K LNG vessel

Cargo compressor room size (meter)	Boundary condition	Leak condition	Numerical setting
28.5 m(W) × 17.5 m(D) × 7.5 m(H)	- Component of leakage Gas: CH_4 - Pressure in: 101,325 Pa - Pressure out: 100,626 Pa - Mass flow in: 305 bar - Leaked gas temperature: 45℃ - Room temperature: 25℃ - Leak rate 1) 0.8 Kg/s, 2) 1.0 Kg/s, 3) 1.25 Kg/s	305 bar (High pressure leak)	- k-ε turbulence model, Realizable - Density based - Scalable wall functions
	- Component of leakage Gas: CH_4 - Pressure in: 101,325 Pa - Pressure out: 100,626 Pa - Mass flow in: 1 bar - Leaked gas temperature: -110℃ - Room temperature: 10℃ - Leak rate 1) 1.8 Kg/s, 2) 3.5 Kg/s,	1 bar (Low pressure leak)	

Corporation (KOGAS). LNG can be obtained from different sources and may have different compositions, implying that the heat value is a variable.

LNG gas dispersion simulations were carried out in a cargo compressor room in accordance with the pinhole sizes, and the boundary condition was set to two (2) "pressure in" natural vents, seventeen (17) "pressure out" mechanical ventilators, and a "mass-flow-inlet" at the leakage points. Moreover, to create a realistic gas dispersion simulation, the actual physical properties of LNG gas were used.

In this research, the LNG gas leak scenarios consisted of a high-pressure leak and a low-pressure leak. Fig. 2 shows the virtual space, which was designed to be 28.5 m (Width) × 17.5 m (Depth) × 7.5 m (Height) based on the arrangement of a 174K LNG vessel equipped with a high-pressure fuel gas compressor for the ME-GI main engines and re-liquefaction equipment. A high-pressure leak was assumed at the high-pressure pump/vaporizer discharge pipe located partially on the deck at the middle of the cargo compressor room (arrow no. 1), and a low-pressure leak was assumed at the vapor return compressor discharge pipe located on the floor deck at the left of the cargo compressor room (arrow no. 3). The leakage scenario for high-pressure gas was considered for three (3) cases, with pinhole diameters of 4.5, 5.0, and 5.6 mm, and the transient flow calculation was carried out until 503s. The low-pressure leakage scenario was composed of two (2) cases, with pinhole diameters of 100 and 140 mm, and a transient flow calculation was carried out until 4,200s.

In Table 2, a pinhole size of 5.6 mm, described in Case 1 ~ 3, was assumed as a rupture case at the maximum capacity of the high-pressure pump/vaporizer, and the pinhole sizes in Case 4-5 are the discharge pipe of the vapor return compressor. One(1) of the gas detection sensors which is the nearest point 30 % LFL (Lower Flammable Limit) of the total four(4) sets was alarmed after the gas leak and then leaked gas was continuously discharged during 10 s and then stopped. Mechanical ventilators were continuously operated before and after the leak, and the methane gas behavior and ventilation capabilities were monitored in this study.

The formulas below are used to estimate the required effective leakage when the flow is subcritical. Under this condition, the formulas (Crowl and Louvar, 1990) used for the calculation of the leaking gas can be assumed to obtain the mass flow rate, *dm/dt*.

$$\frac{dm}{dt} = c_d A_h P_0 K \sqrt{\frac{W_g}{\gamma R T}} \tag{1}$$

Here, *dm/dt*, c_d, A_h, P_0, W_g, , R, and T represent the mass flow rate, leakage coefficient ($c_d = 0.97$), area of the pinhole, internal pressure of the pipe, molecular weight, specific heat ratio (c_p/c_v), gas constant, and gas temperature, respectively. In addition, the constant K in Equation (2) is related to the gas leakage rate.

$$K = \gamma\left(\frac{2}{\gamma+2}\right)^{\frac{\gamma+1}{2(\gamma-2)}} \tag{2}$$

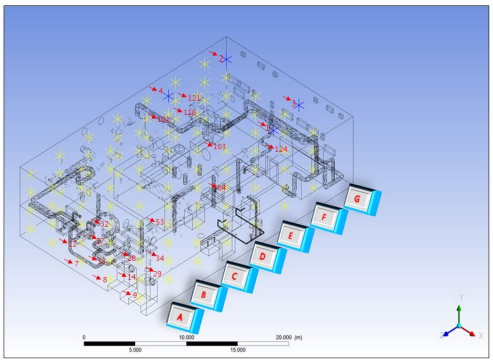

Fig. 2. Real gas detection sensor and virtual monitor points in cargo compressor room of 174K LNG vessel.

In CFD analysis, 'Ansys Fluent Release v17.2' was used as simulation and calculation tool.

Table 2. Mass flow rate for pinhole size variations at 305 bar and 1 bar

	Leak location	Case	Pin hole size	Mass flow rate (kg/s)	Mass flow rate (kg/h)
Scenario 1	Discharge pipe of high- pressure pump/vaporizer (305 bar)	Case 1	4.5 mm	0.8	2,880
		Case 2	5.0 m	1.0	3,600
		Case 3	5.6 mm	1.25	4,500
Scenario 2	Discharge pipe of vapor return compressor (1 bar)	Case 4	100 mm	1.8	6,480
		Case 5	140 mm	3.5	12,600

3. Results and discussion

The position of a gas detector in a hazardous area is very critical since the activation of safety systems and functions requires fast detection of the gas (Luketa-Hanlin et al., 2007). In addition to the recommended detector locations presented in the IGC code provides a table with gas detection main principles covering several areas such as the engine room and the compressor room. This code will not be presented in detail because this paper emphasizes on the factors which must be considered in order to find the optimized detector positions. Bafjord (2011) has examined the most suitable location for gas detection in offshore installations for oil and gas production and evaluated the effects on the functionality and reliability of the gas detection system. Using FLACS, he studied the physical factors that affect the optimum behavior of the exhaust gas with wind speed, wind direction, source of leakage, leakage direction, rate of leakage, gas composition and geometry. Because rapid detection of escape gases is one of the key requirements associated with the gas detection system, the detection time is an important factor in the reliability of the system.

Based on the Fig. 2, a total of 140 virtual points, as defined in Table 3, were selected, excluding real gas detection points 1, 2, 3, and 4. To analyze the CH_4 volume fraction, the number of virtual monitor points was five in the X-direction, four in the Y-direction, and seven in the Z-direction, and the number of virtual monitor points was from 5 to 144. Moreover, the naming in the Z-direction was from A to G, and thus 20 virtual monitor points were composed of seven X-Y planes.

3.1 Scenario 1: Gas detection positions for high-pressure leak

Fig. 3 shows a distribution plot of the CH_4 volume fraction for scenario 1 according to Table 2. The gas detection points made up a total four (4) sets, and a gas detection alarm is sounded at 30 % LFL (0.015). Thus, the gas cloud behavior was between 0.015 (15,000 ppm) to 0.05 (50,000 ppm). Moreover, all cases monitored showed similar gas behavior. A gas cloud was vertically positioned from the pinhole surface of the pipe and dispersed to the ceiling and walls. The gas cloud behavior was captured from the gas detection alarm up to 10s for each case. Their sizes are proportional to the leakage flow rate. All cases reached 30 % LFL (15,000 ppm) within 5s from the leak starting at gas detection point 1, and then gradually decreased, as shown in Fig. 4. The gas leakage stopped after 10s of the alarm. The CH_4 volume fractions at 7 and 1 m planes at the final measuring time all showed lower values of 10,230 ppm. The monitoring values for all gas detection

Table 3. Real gas detection sensor and virtual monitor points in cargo compressor room

Location of real gas detection sensors			
Sensor No.	X(m)	Y(m)	Z(m)
1	13	7	6.5
2	2	7	2
3	12	7	2
4	2	7	10

Location of virtual monitor points						
A (x,y,z)	**B (x,y,z)**	**C (x,y,z)**	**D (x,y,z)**	**E (x,y,z)**	**F (x,y,z)**	**G (x,y,z)**
5(1,1,28)	25(1,1,24)	45(1,1,20)	65(1,1,16)	85(1,1,12)	105(1,1,8)	125(1,1,4)
6(4,1.28)	26(4,1,24)	46(4,1,20)	66(4,1,16)	86(4,1,12)	106(4,1,8)	126(4,1,4)
7(8,1.28)	27(8,1,24)	47(8,1,20)	67(8,1,16)	87(8,1,12)	107(8,1,8)	127(8,1,4)
8(12,1,28)	28(12,1,24)	48(12,1,20)	68(12,1,16)	88(12,1,12)	108(12,1,8)	128(12,1,4)
9(16,1,28)	29(16,1,24)	49(16,1,20)	69(16,1,16)	89(16,1,12)	109(16,1,8)	129(16,1,4)
10(1,3,28)	30(1,3,24)	50(1,3,20)	70(1,3,16)	90(1,3,12)	110(1,3,8)	130(1,3,4)
11(4,3,28)	31(4,3,24)	51(4,3,20)	71(4,3,16)	91(4,3,12)	111(4,3,8)	131(4,3,4)
12(8,3,28)	32(8,3,24)	52(8,3,20)	72(8,3,16)	92(8,3,12)	112(8,3,8)	132(8,3,4)
13(12,3,28)	33(12,3,24)	53(12,3,20)	73(12,3,16)	93(12,3,12)	113(12,3,8)	133(12,3,4)
14(16,3,28)	34(16,3,24)	54(16,3,20)	74(16,3,16)	94(16,3,12)	114(16,3,8)	134(16,3,4)
15(1,5,28)	35(1,5,24)	55(1,5,20)	75(1,5,16)	95(1,5,12)	115(1,5,8)	135(1,5,4)
16(4,5,28)	36(4,5,24)	56(4,5,20)	76(4,5,16)	96(4,5,12)	116(4,5,8)	136(4,5,4)
17(8,5,28)	37(8,5,24)	57(8,5,20)	77(8,5,16)	97(8,5,12)	117(8,5,8)	137(8,5,4)
18(12,5,28)	38(12,5,24)	58(12,5,20)	78(12,5,16)	98(12,5,12)	118(12,5,8)	138(12,5,4)
19(16,5,28)	39(16,5,24)	59(16,5,20)	79(16,5,16)	99(16,5,12)	119(16,5,8)	139(16,5,4)
20(1,7,28)	40(1,7,24)	60(1,7,20)	80(1,7,16)	100(1,7,12)	120(1,7,8)	140(1,7,4)
21(4,7,28)	41(4,7,24)	61(4,7,20)	81(4,7,16)	101(4,7,12)	121(4,7,8)	141(4,7,4)
22(8,7,28)	42(8,7,24)	62(8,7,20)	82(8,7,16)	102(8,7,12)	122(8,7,8)	142(8,7,4)
23(12,7,28)	43(12,7,24)	63(12,7,20)	83(12,7,16)	103(12,7,12)	123(12,7,8)	143(12,7,4)
24(16,7,28)	44(16,7,24)	64(16,7,20)	84(16,7,16)	104(16,7,12)	124(16,7,8)	144(16,7,4)

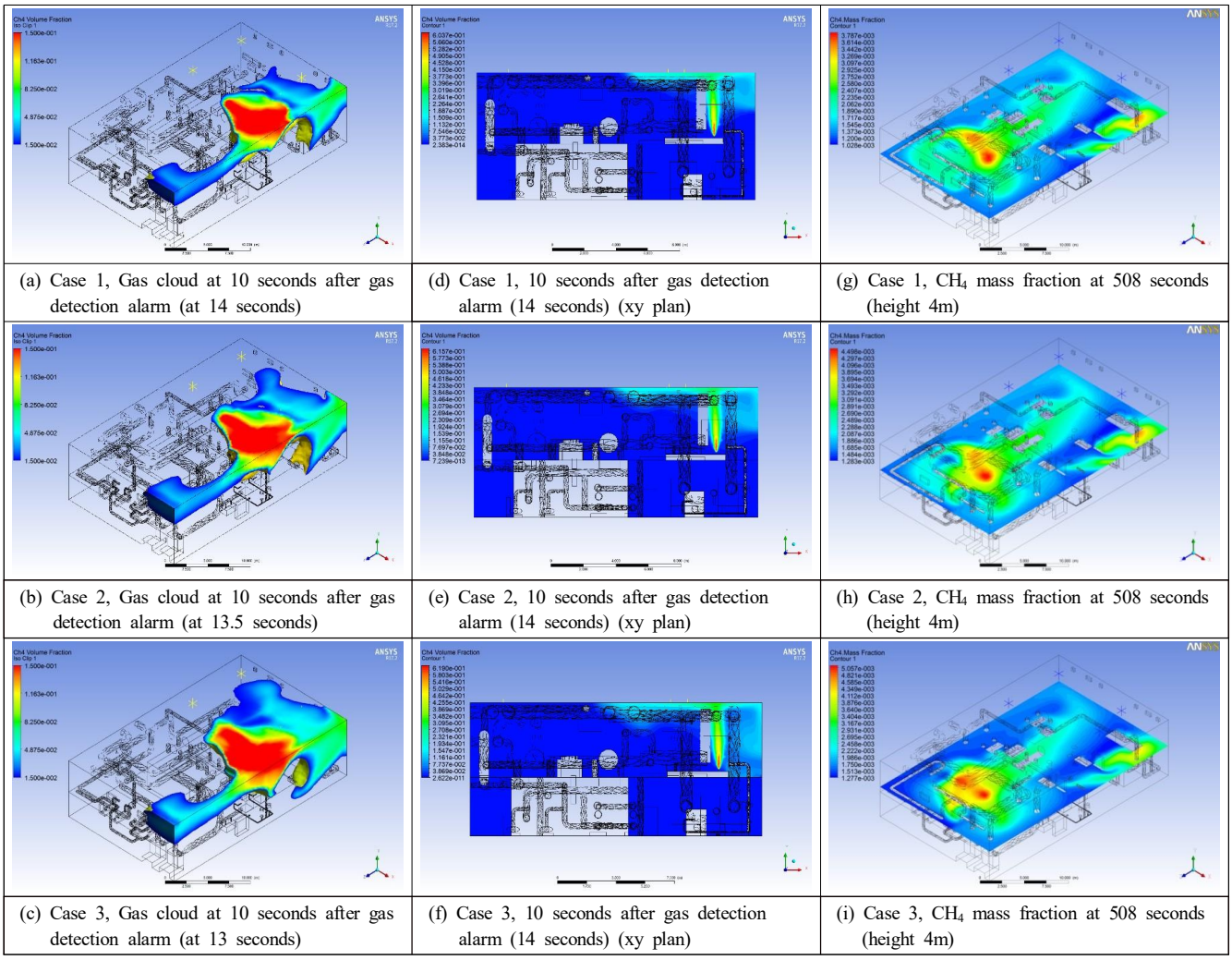

(a) Case 1, Gas cloud at 10 seconds after gas detection alarm (at 14 seconds)

(d) Case 1, 10 seconds after gas detection alarm (14 seconds) (xy plan)

(g) Case 1, CH_4 mass fraction at 508 seconds (height 4m)

(b) Case 2, Gas cloud at 10 seconds after gas detection alarm (at 13.5 seconds)

(e) Case 2, 10 seconds after gas detection alarm (14 seconds) (xy plan)

(h) Case 2, CH_4 mass fraction at 508 seconds (height 4m)

(c) Case 3, Gas cloud at 10 seconds after gas detection alarm (at 13 seconds)

(f) Case 3, 10 seconds after gas detection alarm (14 seconds) (xy plan)

(i) Case 3, CH_4 mass fraction at 508 seconds (height 4m)

Fig. 3. Distribution of CH_4 volume fraction for high pressure leak (Scenario 1).

points remained under 6,500 ppm after 508s. Fig. 5 shows the CH_4 volume fraction at after 10s (a) from the gas detection alarm, and 504s (b) for case 3. As shown in Fig. 4, for a high-pressure leak, the gas behavior for cases 1, 2, and 3 are similar, and thus case 3 with the highest leak rate was analyzed. The highest CH_4 concentration exceeding 80,000 ppm was found at virtual monitor points 84, 103, and 124, and the detected values were between 70,000 and 80,000 ppm. All of these points are located at the highest position, and it was verified that the gas leak at 305 bar under a temperature of 45℃ was distributed to the ceiling because the gas is lighter than air. Points 7, 8, 12, and 13 in Fig. 5(b) are located at the farthest and lowest positions from the ventilators, and they are on the right-hand side of the cargo compressor room because the leak point is located on the right-hand side. Points 32 and 53 are around the high-pressure fuel gas compressor, and it was verified that the remaining gas is not easily ventilated owing to a large obstacle with a size of 3,000 mm × 8,150 mm × 5,000 mm (W × D × H).

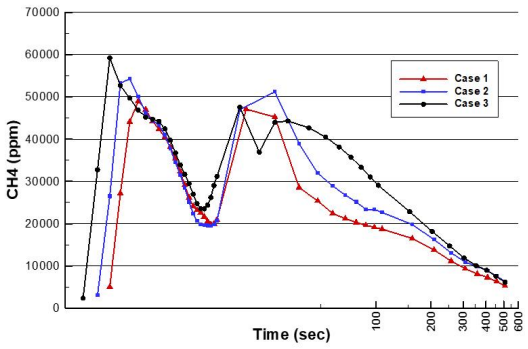

Fig. 4. CH_4 disturibution of 30 % LFLwithin 5s from the leak starting at gas detection point 1 for Scenario 1.

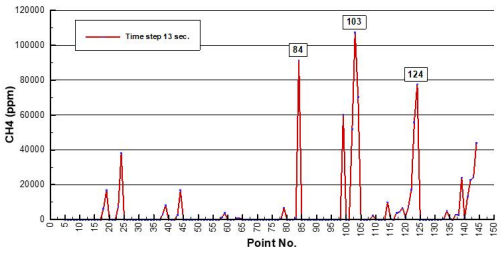

(a) CH_4 volume fraction (ppm) after 10 seconds from gas detection alarm (Case 3)

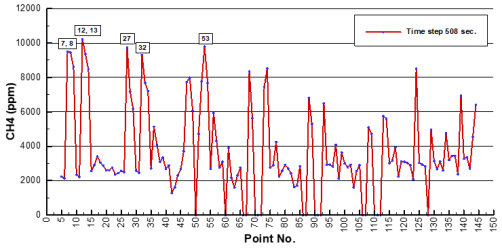

(b) CH_4 volume fraction (ppm) at 508s (Case 3)

Fig. 5. CH_4 volume fraction at after 10s from the gas detection alarm and 508s for case 3 (high-pressure leak, Section 1).

3.2 Scenario 2: Gas detection positions for low-pressure leak

The gas leak continued for 10s after the gas alarm sounded and stopped, after which only the mechanical ventilators were operated without a gas leak. The first gas detection alarm was first monitored at location no. 1 for cases 4 and 5, as shown in Fig. 6. Moreover, the highest CH_4 volume fraction at 10 s after the alarm was monitored at location no. 1 location for all cases. The final measurements at 2,312 and 4,697s for each case were conducted without the flammable concentration, and all measured values continued to be below 9,000 ppm. The leakage flow rate of case 5 is nearly two (2) times more than that of case 4, and it takes nearly two (2) times the time to ven comparing the final measurement time between cases 4 and 5. The transient calculation of case 5 is 1,910s, which is much more than in case 4.

Fig. 6 and 7 show distribution of the CH_4 volume fraction for scenario 2 of Table 2. The gas detection points and gas cloud were assumed to be the same as applied with the high-pressure leak, as already described. In Fig. 8, the gas cloud is vertically positioned from the pinhole surface of the pipe and dispersed to the ceiling and walls. The leak point is located partially under the deck, and the gas temperature inside the pipe is approximately -110℃. Thus, a comparatively heavier gas than a high-pressurized gas leak with a temperature of 43℃ at 305 bar cannot be easily dispersed to other spaces, and a dense high-flammable gas was found partially under the deck farthest from the ventilators. The gas cloud behavior was captured from the gas detection alarm up to 10s after the gas leak. Their sizes are proportional to the leak flow rate. The flammable gas cloud for two (2) cases between 50,000 and 150,000 ppm, at 500s in Fig. 7 (a) and 900s in Fig. 7 (b), shows separate plots, which remain at the farthest area from the mechanical ventilators. These areas are regarded as an accumulated flammable gas area, and thus we confirmed that additional gas detection devices are needed. All two (2) cases reached 30 % LFL (15,000 ppm) within 80 and 65s from the start of the leak, and there was no flammable gas cloud for the monitored gas detection points, after which the CH_4 volume fraction gradually decreased. In cases 4 and 5, the values are significantly decreased after 900 and 1,320s, respectively. The CH_4 volume fractions shown in Fig. 7(e) and (f) at 4 m are all lower values of 10,000 ppm.

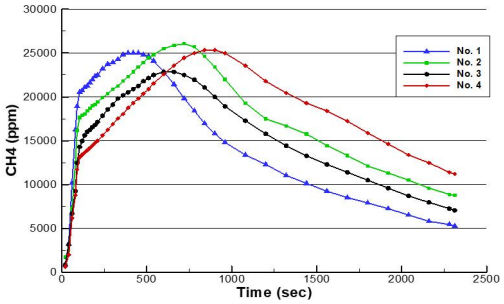

(a) CH_4 volume fraction variation at gas detection point for case 4

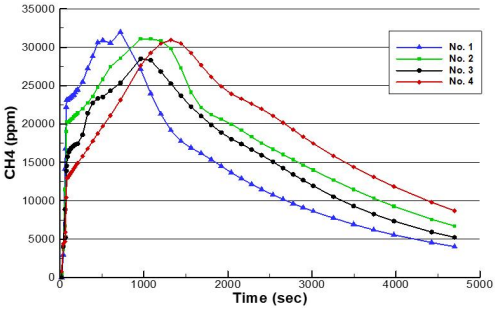

(b) CH_4 volume fraction variation at gas detection point for case 5

Fig. 6. CH_4 volume fraction profiles for low-poressure leak (Scenario 2).

Fig. 8(a) shows the CH_4 volume fraction at a gas alarm point (80s), 10s after the gas detection alarm (90s), and at 900s for Case 4. The highest CH_4 concentration at 80 and 90s is between 250,000 and 450,000 ppm for virtual monitor points 8, 13, 29, and

34. All of these points are located around the leaked position and at the farthest and lowest positions from the ventilators partially under the deck. It was verified that the leaked gas of 1 bar at -110℃ was distributed to the lowest position because it is heavier than the air. Points 46, 51, 65 and 85 with the highest CH_4 concentration exceeding 25,000 ppm at 900s are located at the farthest and lowest positions from the ventilators. Points 101, 116, and 121 show the highest CH_4 concentration at 2,312s, the values of which are between 12,000 and 14,000 ppm, as shown in Fig. 8(b). They are around the high-pressure fuel gas compressor, and it was also verified that the remaining gas is not easily ventilated the same as a high-pressure leak.

Fig. 9(a) shows the CH_4 volume fraction at a gas alarm point (65s), at 10s after gas detection alarm (75s), and at 1320s for Case 2. The highest CH_4 concentration at 65 and 75s is between 350,000 and 450,000 ppm at virtual monitor points 9, 14, 29, and 34. All of these points are located around the leaked position and at the farthest and lowest positions from the ventilators partially under the deck, similar to case 4. Points 45, 46, 51, 65 and 85 with the highest CH_4 concentration at 1320s are between 35,000 ppm and located at the farthest and lowest positions from the ventilators. In Fig. 9(b), points 101, 116, and 124 show the highest CH_4 concentration at 4,697s, with values of between 8,000 and 10,000 ppm. They are around the high-pressure fuel gas compressor, and the remaining gas was mainly accumulated the same as the high-pressure leak, and as low-pressure leak of case 4.

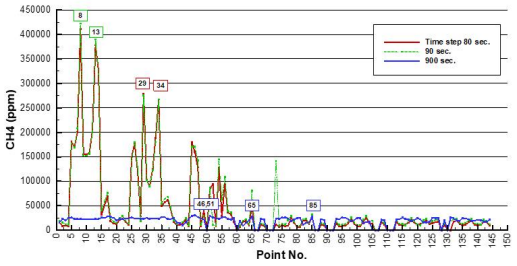

(a) CH_4 volume fraction (ppm) variation for low-pressure leak (case 4)

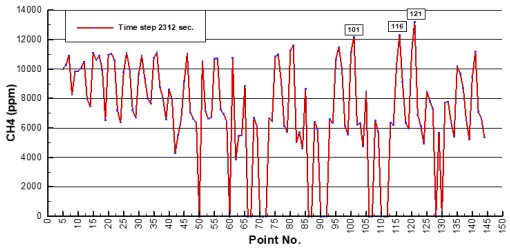

(b) CH_4 volume fraction (ppm) variation at 2,294s for low-pressure leak (Case 4)

Fig. 8. CH_4 volume fraction profiles for low-pressure leak (Case 4).

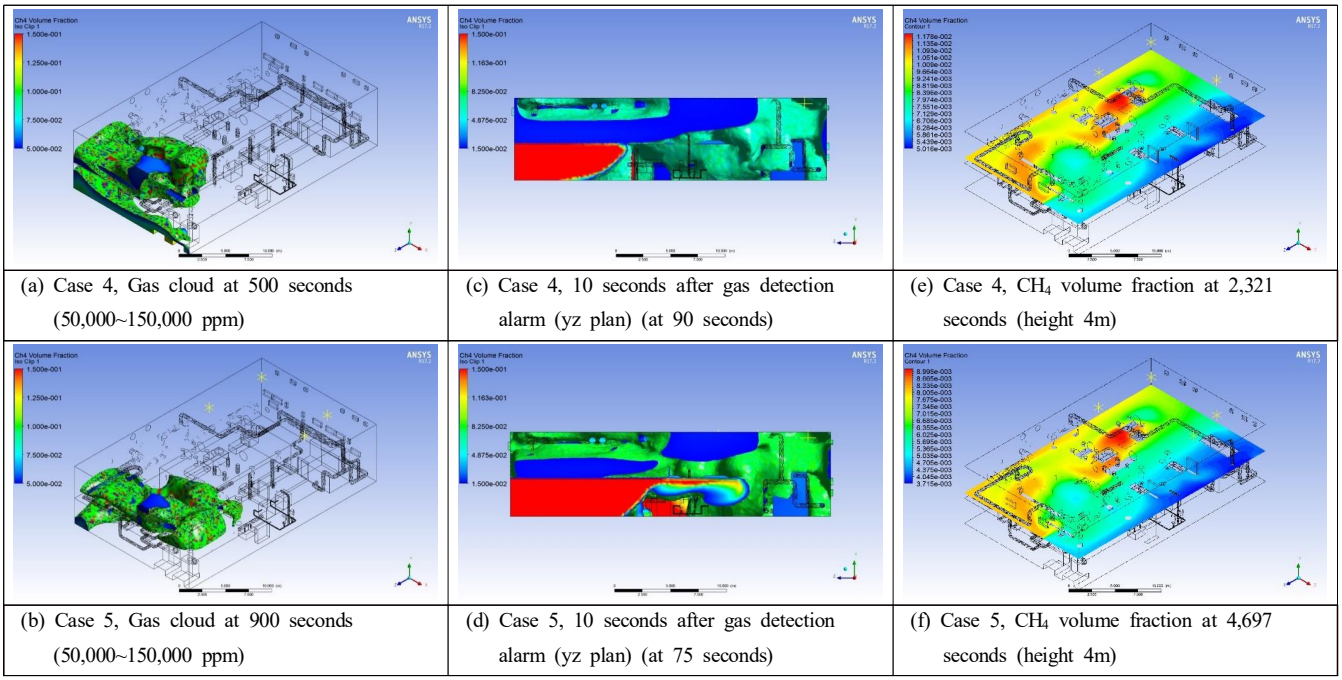

(a) Case 4, Gas cloud at 500 seconds (50,000~150,000 ppm)

(c) Case 4, 10 seconds after gas detection alarm (yz plan) (at 90 seconds)

(e) Case 4, CH_4 volume fraction at 2,321 seconds (height 4m)

(b) Case 5, Gas cloud at 900 seconds (50,000~150,000 ppm)

(d) Case 5, 10 seconds after gas detection alarm (yz plan) (at 75 seconds)

(f) Case 5, CH_4 volume fraction at 4,697 seconds (height 4m)

Fig. 7. Distribution of CH_4 volume fraction for low-pressure leak (Scenario 2).

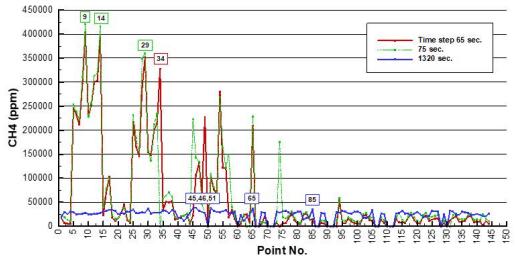

(a) CH_4 volume fraction (ppm) variation for low-pressure leak (case 5)

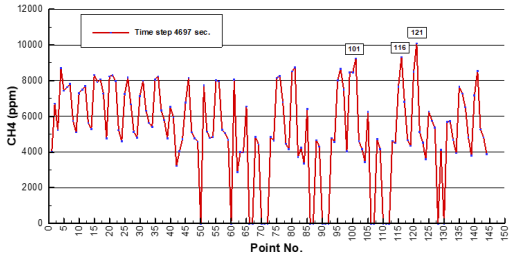

(b) CH_4 volume fraction (ppm) variation at 2,294s for low-pressure leak (Case 5)

Fig. 9. CH_4 volume fraction profiles for low-pressure leak (Case 5).

4. Conclusion

The position of gas detectors affect the time from a gas leak starts until the escaped gas is detected. Potential leak locations and directions of air currents should be taken into consideration before detector positions are determined.

According to the Facility Regulations (PSA, 2011) the placement of detectors shall be based on relevant scenarios and simulations or tests. The use of CFD simulations is one way to find the best suited gas detector positions. Requirements such as fast and reliable detection are strongly influenced by the position of the gas detectors.

The LNG gas leak and dispersion were analyzed at high and low pressures according to the pinhole size for a cargo compressor room of a 174K ME-GI LNG vessel. Scenarios for a gas leak were examined for high pressure at 305 bar and for low pressure at 1 bar. High-pressure gas leak scenarios were examined for 4.5, 5.0, and 5.6 mm pinhole sizes (case 1~3), and low-pressure leak scenarios were examined for 100 and 140 mm pinhole sizes (case 4 and 5). Transient gas simulations were adopted to obtain the values of various time steps.

Through this study, we identified the ventilation capability with relatively cold and heavy LNG gas from low pressure partially under the deck and compared it with hot and light LNG gas at high pressure. The quantitative data obtained through the numerical simulation will help our understanding of the risk factors based on the flow characteristics of not only an ME-GI LNG ship but also similar ships. High-pressure gas leak scenarios show that the cargo compressor room of a 174K ME-GI LNG will not pose a serious risk problem regarding the flammable gas concentration because a ventilation assessment for a 5.6-mm pinhole size as the gas rupture condition was verified. Low-pressure gas leak scenarios show that the flow rate of a leak for case 2 was nearly two (2) times greater than that of case 4. Case 5 takes nearly twice the time of case 1 to ventilate the CH_4 gas for all gas detection points when comparing the final measurement time. The ventilation time of case 5 is much more 1,910s than in case 1. Thus, the more leakage gas that is present, the more time it takes to ventilate the gas.

Moreover, in the case of a high-pressure gas leak and dispersion, real gas detection sensors should be moved to the right-hand side of the cargo compressor room at around the ceiling height. In addition, in the case of a low-pressure leak and dispersion, CH_4 gas is not easily ventilated partially under the deck and in front of the high-pressure fuel gas compressor. Therefore, it was identified that additional gas detection sensors should be applied, or existing gas sensors should be moved to these points.

Acknowledgments

This work was part of “Test evaluation for LNG bunkering equipment and development of test technology” supported by the Ministry of Oceans and Fisheries (Grant No. 20180048), and the “Development of module construction technology and core equipment packages for topside module commercialization (over 500 tons)” supported by the Ministry of Trade, Industry and Energy of Korea government (Grant No. 10085629).

References

[1] Bafjord, J. A.(2011), Positioning of gas detectors at offshore installations, M.D. University of Stavanger, Norway.

[2] Bengtsson, S., K. Andersson and E. A. Fridell(2011), A comparative life cycle assessment of marine fuels: liquefied natural gas and three other fossil fuels, Proc IMechE, Part M. J. Eng Maritime Environ. 225, 97-110.

[3] Burel, F., R. Taccani and N. Zuliani(2013), Improving sustainability of maritime transport through utilization of

Liquefied Natural Gas (LNG) for propulsion. Energy. Vol. 57, pp. 412-420.

[4] Chang, D., T. Rhee, K. Nam, K. Chang, D. Lee and S. Jeong(2008), A study on availability and safety of new propulsion systems for LNG carriers, Reliability Engineering and System Safety. Vol. 93, pp. 1877-1885.

[5] Crowl, D. A. and J. F. Louvar(1990), Chemical process safety: Fundamentals with applications, Prentice Hall PTR, New Jersey.

[6] GECF, Gas basic(2013), Environment, https://www.gecf.org/gas-data/environment.aspx.

[7] Hoenders, R.(2013), EU initiatives regarding the use of LNG as bunker fuel and EMSA's involvement in promoting the use of LNG as alternative fuel. European Maritime Safety Agency (EMSA), Lisbon.

[8] IMO, IGC code(2016)

[9] IMO, Resolution MEPC.212(63)(2012a), Guidelines on the method of calculation of the attained energy efficiency design index (EEDI) for new ships, MEPC 63/23. International Maritime Organization, London.

[10] IMO, Resolution MEPC.212(63)(2012b), Guidelines for the development of a ship energy efficiency management plan (SEEMP), MEPC 63/23. International Maritime Organization, London.

[11] Kang, H. K.(2012), An examination on the dispersion characteristics of boil-off gas in vent mast exit of membrane type LNG carriers, Journal of the Korean Society of Marine Environment & Safety, Vol. 19(2), pp. 225-231.

[12] Luketa-Hanlin, A., R. P. Koopman and D. L. Ermak(2007), On the application of computational fluid dynamics codes for liquefied natural gas dispersion, Journal of Hazardous Materials, Vol. 140(3), pp. 504-517.

[13] MAN B&W Diesel(2006), Dual fuel concept: Analysis of fires and explosions in engine room, Report for MAN B&W Diesel A/s, Report no. 2006-0897.

[14] Paltrinieri, N., A. Tugnoli and V. Cozzani(2015), Hazard identification for innovative LNG regasification technologies, Reliability Engineering and System Safety, Vol. 137, pp. 18-28.

[15] PSA(2011), Petroleum Safety Authority, Framework HSE, Management and Facilities Regulations, Norway. Available from: http://www.ptil.no/regulations/category216.html.

Received : 2019. 06. 18.
Revised : 2019. 08. 26.
Accepted : 2019. 08. 28.